# Configurational stability and magnetization processes in submicron permalloy disks

Jonathan Kin Ha,* Riccardo Hertel, and J. Kirschner
*Max-Planck-Institut für Mikrostrukturphysik, Weinberg 2, 06120 Halle, Germany*
(Received 8 August 2002; published 27 February 2003)

A finite-element micromagnetic approach is employed to study magnetization reversal processes in submicron permalloy disks of various sizes, with diameter between 50 and 500 nm and thickness between 5 and 200 nm. The reversal is accomplished by a fixed-directional in-plane magnetic field. Depending on which (meta)stable states are accessible in the magnetization path, various types of hysteresis loops are observed. For example, for thin disks ($<5$ nm), the magnetization remains in an ''onion'' (almost a single-domain) state throughout the process, resulting in a square loop. For thick disks ($>50$ nm), the magnetization collapses to a vortex state, resulting in a dumbbell-looking loop. For disks whose diameters are larger than 200 nm, the magnetization can pass through some intermediate buckle state before collapsing to either a vortex or an onion state. In all cases, the reversal process is dictated by the stability of the magnetic configuration. For some disks, a rotational field is used effectively to reverse the magnetization and hence avoid the so-called configurational anisotropy effect. The spread function is introduced to quantify the degree of nonuniformity of a magnetic configuration. This quantity is particularly helpful in studying the evolution of a magnetic pattern by the action of an external field.

DOI: 10.1103/PhysRevB.67.064418 PACS number(s): 75.40.Mg, 75.60.Ch, 75.60.Jk

## I. INTRODUCTION

The so-called configurational anisotropy was introduced by Schabes and Bertram[1] in 1988 to explain the enhanced switching field in their simulated magnetic cubes (it was higher than that predicted by the Stoner-Wohlfarth model[2]). It was argued that this larger field, the field needed to induce an irreversible jump to the reversed state, was due to the inherent property of the nonuniform magnetic pattern and could be thought of as that from an anisotropy insofar as the magnetization process was concerned. But the association of this effect to an anisotropy is problematic because it does not play a role in determining the spin arrangement of the ferromagnet (which is more a consequence of it), as does any true source, such as that of crystalline or shape. Perhaps it would have been more accurate to call it *configurational stability*—and is so named hereafter—because it is really about the stability of a magnetic configuration, the barrier which the external magnetic field needs to overcome to reverse the direction of the magnetization. It should be made clear that the above-mentioned stability refers to that against the external magnetic field, and *not* that of, say, thermal disturbance, for example.

Undoubtedly, configurational stability is the key in understanding magnetization processes in submicron ferromagnetic elements. The spins in such a confined geometric structure arrange in a *single*, nonuniform pattern, like that of a flower,[1] *C*,[3] or vortex state,[4] rather than in an aggregate of uniform magnetization or domains commonly seen in bulks and unpatterned thin films,[21] like that of the Landau pattern.[5] The adoption of a nonuniform magnetic pattern can give rise to stability against the external field, as this will be explained and illustrated in detail later in the paper. The important message here, as part of the Introduction, is this: Unlike that in a bulk sample in which the magnetization process is dominated by either wall motion or spin rotation or a combination of these two mechanisms,[2,6] it is the stability of the configuration that dictates the magnetization process in a submicron element.

More specifically, this paper is about magnetization reversal processes in submicron permalloy disks using Brown's *static* micromagnetic approach.[7] The circular shape is opted to eliminate any in-plane shape anisotropy effect. This and the exclusion of any intrinsic anisotropy in the permalloy are efforts to show the effect of the configurational stability as simply and clearly as possible. The reversal process begins with the magnetization in saturation along the external magnetic field applied in the disk plane. The field direction remains fixed throughout the magnetization process, but its magnitude decreases and then increases in the direction of opposite polarity, typically in a step size of a few milli-tesla field or less. Depending on the sample size, different types of hysteresis loops are observed due to the presence of different magnetic configurations in the magnetization process. In some disks, a rotational field of constant amplitude is used instead for the reversal, and it has been proved successful in avoiding a certain magnetic configuration which would be undesirable for certain applications, even for the simple reason that it would otherwise take too large of a field to overcome the stability of the configuration. To quantitatively measure the degree of nonuniformity of a magnetic configuration, the spread function (SF) is introduced and is particularly useful in tracking the evolution of a magnetic pattern by the action of the external field.

Another point worth mentioning here is that the study of the magnetization processes in submicron elements is currently a hot research topic. It has received much attention, particularly in the past few years from both experimentalists and theoreticians, and rightly so for many reasons, among which are that (i) these magnetization processes represent a new genre of magnetization process for the reason mentioned above and hence are interesting in themselves, (ii) the precise control of the magnetization process is crucial in the operation of a spin-electronic device such as magnetic read

 

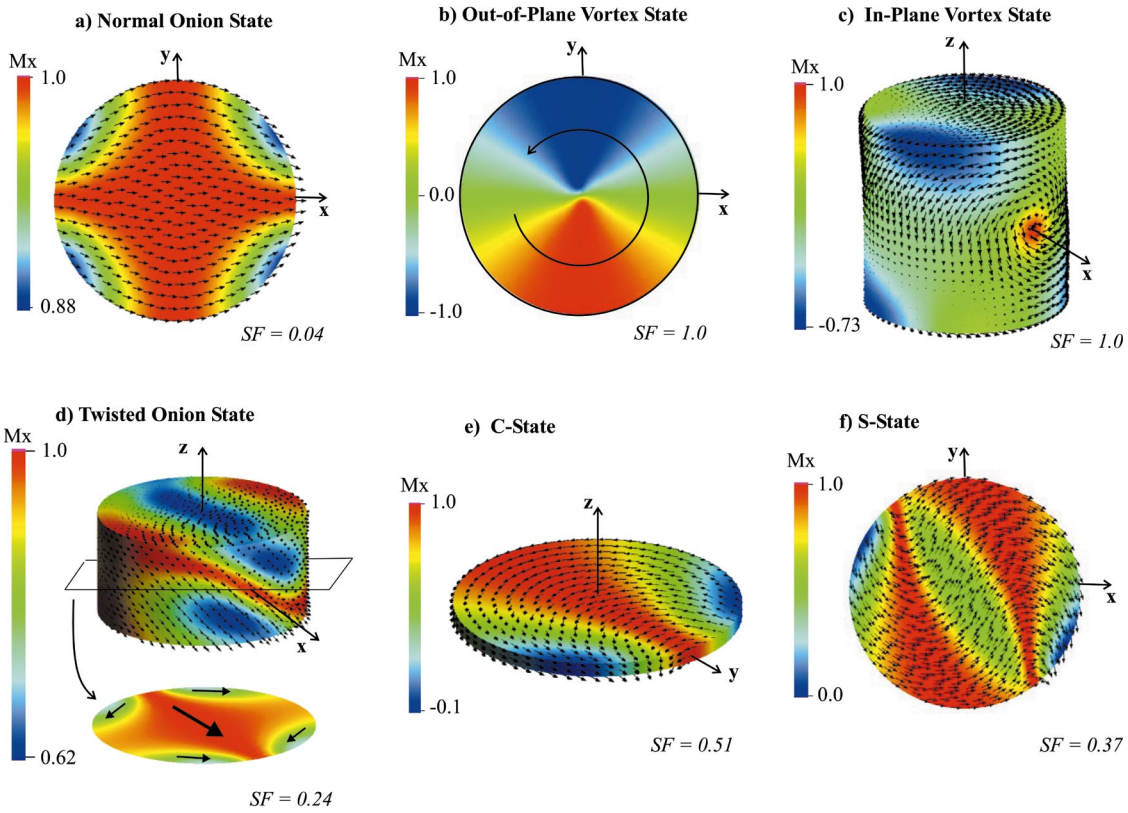


FIG. 1. (Color) Magnetic configurations observed in submicron permalloy disks. The notation such as D200R20 is used to specify the disk size. For example, D200R20 means that the disk diameter is 200 nm and its diameter-to-thickness ratio $d/t$ is 20. On the bottom right-hand corner of each configuration is the corresponding spread function SF value. (a) Onion state seen in D200R20 at 10 mT, (b) out-of-plane vortex state in D400R10 at zero field, (c) in-plane vortex state in D100R1 at zero field, (d) twisted onion state in D200R2 at 162 mT, (e) *C* state in D200R20 at zero field, and (f) *S* state in D500R30 at 4 mT field.

head or magnetic random memory access (MRAM), and (iii) submicron elements are potential candidates for ultrahigh-density data storage.[3,8,9]

## II. NUMERICAL METHOD AND SAMPLE SPECIFICATIONS

The numerical approach, based on the hybrid finite-element–boundary-integral method (FEM-BIM),[10] is employed to study the nonuniform arrangement of the magnetization. The energy of the system is modeled to include the exchange, stray field, and Zeeman terms. An equilibrium magnetic configuration is obtained by seeking a minimum in the total energy of the system. The minimization is achieved self-consistently; that is, the stray field is first calculated using an assumed magnetic configuration and is subsequently treated as an external field source. The assumed magnetic structure is then allowed to relax, via a conjugate gradient path, to a new minimum-energy configuration from which the stray field is recalculated. The process is repeated until the energy difference between that before and after the minimization is within some specified tolerance. Further discussion of the numerical method can be found in Ref. 11.

The disk material properties are taken to be those of isotropic permalloy, as mentioned in the Introduction. More specifically, the saturation magnetization value of 1 T and exchange stiffness constant of $1.3\times10^{-11}$ J/m are used in the calculation. These parameters give the exchange length of 5.7 nm. In this paper, the exchange length is defined as $L_{ex}\equiv\sqrt{A/k_d}$ where $k_d=J_s^2/2\mu_0$ is the stray field constant with $J_s=|\mathbf{J_s}|$ being the magnitude of the magnetization vector. The disk diameter is varied from 50 to 500 nm and the thickness from 5 to 200 nm. The notation used to specify the disk size is best illustrated by an example: D200R10 means a disk with a diameter of 200 nm and diameter-to-thickness ratio $d/t$ of 10. Also, to facilitate the discussion below, a Cartesian coordinate system is introduced with the $x$ axis oriented along the applied field direction; the $z$ axis is the disk normal.

## III. MAGNETIC CONFIGURATIONS

Before the numerical results are presented, it is important to introduce each of the different magnetic configurations encountered during the magnetization processes, for this knowledge is needed to understand the stability of the spin arrangement against the applied external field and for the simple reason of giving a visual link between the pattern and its name. In this section, a brief discussion of the magnetic structures is presented. A more detailed description can be found in another paper.[12]

Figure 1 shows a representative of each of the different

magnetic configurations observed in various disks. The normal onion state[22] has a clear in-plane magnetic axis of symmetry, which we call the onion axis. Along this axis, the magnetization is quite uniform, but some curling is observed in the regions [marked by blue color in Fig. 1(a)] located near the perimeter at about $\pm 45°$ from this onion axis. This tendency for the magnetization to lie along the disk edge stems from the need to minimize the amount of surface poles, which is defined by the dot product $\vec{M} \cdot \hat{n}$ where $\hat{n}$ is the normal unit vector. Although not shown in the figure, there is some opening and closing (i.e., flowering) of the magnetization at the two ends of the symmetry axis near the top and bottom surfaces of the disk. This provides a flux closure path for the stray field outside the sample. In thicker disks, instead of flowering, it is energetically more favorable for the perpendicular component of the magnetization to have some flux closure arrangement, resulting in what we call a twisted onion state [Fig. 1(d)]. In this state, the direction of the onion axis is being twisted as it proceeds away from the central plane of the disk, and hence the name twisted onion state is used to describe the magnetic pattern.

In a vortex state, the magnetization aligns with the geometry of the disk as much as possible to achieve a flux closure condition. This is done at great expense of the exchange energy. Two types of vortices are observed. They are out-of-plane and in-plane vortices [see Figs. 1(b) and 1(c), respectively], depending on whether the axis of the vortex core points out of or in the disk plane, respectively. The out-of-plane vortex state is the more common of the two and has been reported in many publications in the literature (e.g., Refs. 4 and 13). However, as far as we know, there have been no reports on the observation of an in-plane vortex state in cylindrical disks, neither experimental nor theoretical.

While the structure of an onion state (normal or twisted) is dominated by the minimization of the exchange energy and that of a vortex state (out of plane or in plane) by the stray field energy minimization, a buckle state is a result of the compromise between the two driving forces. Consequently, the magnetic pattern is neither as uniform as that in the onion state nor as spread as in that of a vortex state. Various degrees of buckling can be identified based on the number of ''oscillation'' it exhibits in the pattern. Buckle states of first and second order are shown in Figs. 1(e) and 1(f), and they are, respectively, called *C* and *S* states, because of their resemblance to the letters of the Latin alphabet. Higher-order buckle states can be observed in larger disks (disks whose diameter is larger than 500 nm), but they will not be discussed in this paper.

## IV. SPREAD FUNCTION

Still another digression is needed before the results on the magnetization processes can be effectively shown. While it is self-evident that the magnetization in an onion state is the least spread or most uniform among the magnetic configurations illustrated in Fig. 1, it is difficult to judge which, among configurationally identical states (such as onions), has the most nonuniform spin arrangement. Hence, it is desirable to have a scalar quantity that would aid us in this effort. And such a quantity would be helpful in tracking the evolution of a magnetic configuration under the action of an external magnetic field. For this reason, the spread function SF is introduced and defined as

$$\mathrm{SF} = 1 - \langle m_x \rangle^2 - \langle m_y \rangle^2 - \langle m_z \rangle^2, \tag{1}$$

where $\langle m_x \rangle^2$, $\langle m_y \rangle^2$, and $\langle m_x \rangle^2$ are the square of the average magnetization components along the *x*, *y*, and *z* directions, respectively. It is not difficult to prove that SF is a real-valued function whose range lies in the *closed* interval $[0, +1]$ (see the Appendix); that is, it maps the information on the nonuniformity of a domain pattern to a real number ranging between 0 and 1, inclusively. If the magnetization is perfectly uniform, $\mathrm{SF} = 0$. If the magnetization is evenly distributed in all directions, $\mathrm{SF} = 1$.

To give the reader a good sense of the spread function, Fig. 1 also shows its value for each of the magnetic configurations. As expected, the onion state gives an almost zero spread value, while that for the two vortices is essentially 1. The two buckle states show intermediate spread values.

The so-called vorticity function has also been used in the literature[1,14,15] to measure the degree of curling of a vortex state in cube-shaped elements. It is defined as the line integral of the tangential magnetization on the edges of the cube normalized to the length of the path. Note that the vorticity is path dependent. On the contrary, the spread function is a global quantity that gives an average spreading of the sample magnetization. Further, it is more versatile in that it can be used to measure the spreading in any magnetic configuration, not just in that of a vortex state.

## V. MAGNETIC HYSTERESIS LOOPS

In this section, the discussion is restricted to the magnetization reversal processes achieved by a bidirectional in-plane magnetic field (as opposed to that of a rotational field to be discussed in the next section). The average magnetization vector is computed by taking the vectorial sum of the magnetization at each node, the contribution of which is proportionally weighted by the assigned nodal volume in the finite-element partition. Its projection onto the applied field direction is plotted for a number of representative disks as a function of the external field. Also shown are the corresponding spread value and relevant energy terms, to shed some respective insight into the evolution and the driving force of the spin rearrangement induced by the external field.

Since it is only necessary to discuss one branch of the hysteresis, we choose the branch that goes from positive to negative field for all the discussions below. For example, if it is said that the magnetization switches at $-10$ mT field, it is meant that the field starts from a positive field and then changes its polarity to $-10$ mT, at which the magnetization of the disk switches.

### A. Onion-to-onion transition

The simplest of all the hysteresis loops observed in these submicron disks is that of a square shape, an example of which, taken from D100R20, is shown in Fig. 2. The switch-

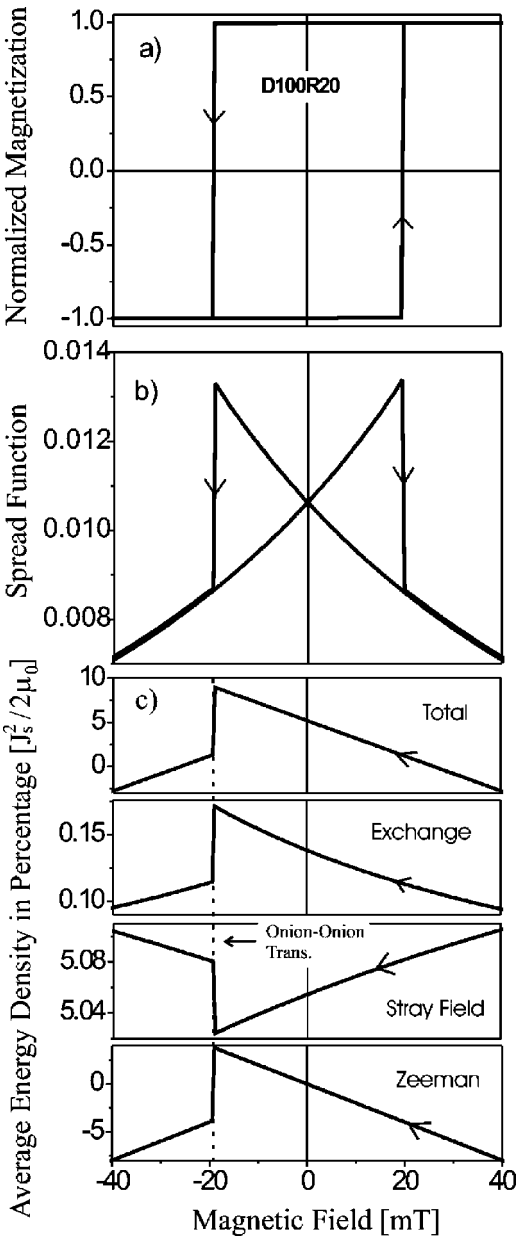


FIG. 2. (a) The average magnetization, (b) spread function, and (c) the relevant energy terms are all plotted as a function of the in-plane magnetic field for D100R20 (diameter=100 nm, diameter-to-thickness ratio $d/t=20$). All the energy terms are normalized to the stray field energy coefficient $K_d=J_s^2/2\mu_0$, where $J_s$ is the saturation magnetization and $\mu_0$ the vacuum permeability constant. Note that only one branch of the hysteresis is shown in the energy plot.

ing occurs at about $-18$ mT. This might strike a dissonant chord in the reader's intuition as being large, considering that the ferromagnetic disk possesses neither intrinsic nor any in-plane shape anisotropies. But in light of what was discussed earlier about the configurational stability effect, this is not so strange after all: the 18 mT field strength is what it takes to destabilize the onion configuration with the magnetic field applied directly opposite to the onion axis. To gather evidence supporting this interpretation, a similar calculation is performed on the same disk except this time with a 400 times stiffer exchange constant, namely, $A=5.2\times10^{-9}$ J/m. This value of $A$ gives the exchange length of 114 nm (as opposed to 5.7 nm if using the true permalloy exchange constant), a length scale that is comparable to the disk diameter. From this, it can be expected that the disk behaves essentially like a single-domain particle because any deviation from uniform magnetization would cause too much exchange energy. The simulation shows the magnetization reverses at about $-0.8$ mT, a much smaller field than what was needed before, and the spread function reads less than $2\times10^{-6}$ throughout the reversal process. Another exploratory calculation is also undertaken, this time with the exclusion of any stray field effect to ensure perfect uniformity in the magnetic pattern (with the exchange stiffness constant $A=1.3\times10^{-11}$ J/m). The result shows that the magnetization switches practically at zero field. This is expected because the disk is modeled to possess no intrinsic magnetic anisotropy. Also, the fact that the spread function is less than $3\times10^{-10}$ at all field strengths (which is within numerical errors of the code) is an attestation that the disk is indeed a single-domain particle. In short, the simulation results suggest strongly that the stability of the onion configuration is responsible for the large switching field in this particular sample. It should be kept in mind that the large switching field observed in the simulation may not be obtainable in experiments due to many factors including (i) the presence of thermal fluctuation that can marginalize the stability of the magnetic configuration and (ii) structural defects such as that the disk perimeter is a bit jagged and hence may provide unintended nucleation sites from which the reversal process can originate.[9,16]

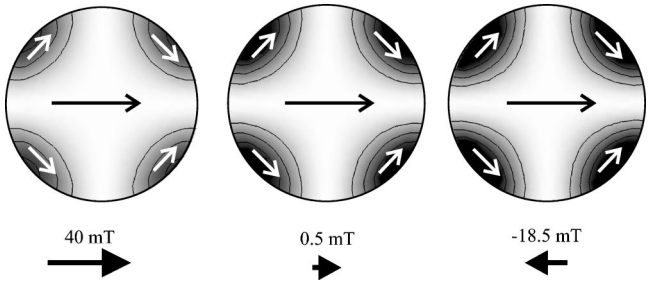


FIG. 3. Density plots of the $x$ component of the average magnetization of D100R20 (diameter=100 nm, diameter-to-thickness ratio $d/t=20$) at 40, 0.5, and $-18.5$ mT field. The lightest region corresponds to $m_x=1$, the darkest to $m_x=0.98$. The contour lines are lines of constant $m_x$ with $m_x=0.995$, 0.990, and 0.985. The arrows on the disk are sketches of the direction of the magnetization in the area. Note that the canting of the magnetization illustrated by the arrows is exaggerated in the figure.

Onto the discussion of the magnetic states encountered during the reversal process, examination of the magnetic configuration shows that the disk remains in a normal onion state in the field range between $\pm40$ mT. The irreversible jump in the magnetization, which occurs at $-18.5$ mT field, corresponds to the transition from one onion state to another of opposite polarity—that is, into another onion state with its axis pointing in the opposite direction. Before the transition, the spread function, as shown in Fig. 2(b), shows that the

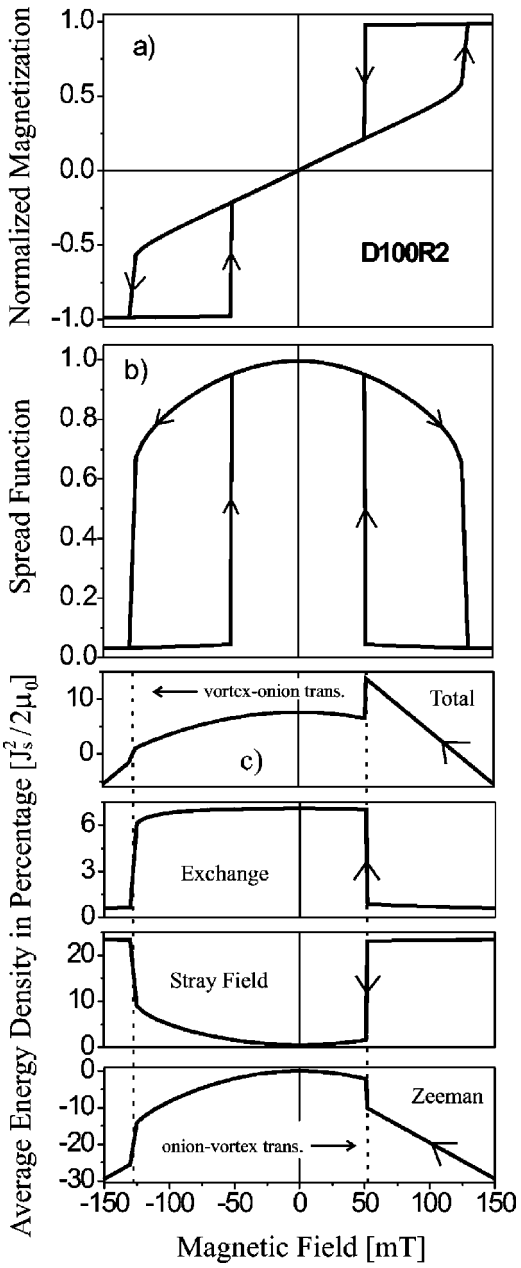


FIG. 4. D100R2 (diameter=100 nm, diameter-to-thickness ratio $d/t=2$): (a) in-plane hysteresis loop; (b) and (c) are the respective spread function and energy terms plotted as a function of the applied field. The magnetization process involves transitions between a normal onion and an out-of-plane vortex states.

magnetization becomes more nonuniform as the field approaches the switching field. But in what manner does the magnetic pattern become more dispersed? This question can be answered by examining the configuration at different magnetic fields. Figure 3 shows three snapshots of the $x$ component of the configuration at saturation (40 mT), near remanence (0.5 mT), and just before the reversal ($-18.5$ mT). Clearly, as the external field decreases, the magnetization becomes more closing up or ''onionated'' in the disk plane, as it is evident by the growing of the region at about $\pm 45°$ away from the direction of the symmetry axis (the dark areas shown in Fig. 3). The magnetization reverses when the barrier separating the two onion states is reduced to zero by the action of the external field. The onion-to-onion transition occurs so as to save both the Zeeman and exchange energies as clearly shown in Fig. 2(c).

### B. Transition between normal onion and out-of-plane vortex states

Another commonly observed type of hysteresis loops is that involving transitions between onion and out-of-plane vortex states. Figure 4(a) shows such a hysteresis loop taken from D100R2. The reversal process goes as follows: the magnetization begins in saturation by a large external field applied in the disk plane. As the field strength decreases, the magnetic pattern evolves continuously to onion states of increasing onionicity—that is, states whose magnetization becomes more closing up toward the onion axis, as that discussed earlier in D100R20. However, at 51 mT field, the onion state collapses, quite abruptly, to a vortex state, resulting in a significant drop in the magnetization component along the field direction and an almost full-scaled jump in the spread function from 0 to 1. The transition is driven purely by the saving of the stray field energy at the expense of both the exchange and Zeeman energies, as shown in Fig. 4(c). Further decrease in the field moves the vortex core in a direction perpendicular to the field, in the manner as such domains aligned with the field grow, those opposed to it shrink, until the field reaches $-128$ mT at which the vortex is annihilated and transformed into another onion state whose axis points along the field direction. This transition is driven by the saving of the Zeeman and exchange energies at the expense of the stray field. Clearly, a much larger field is needed to reverse the magnetization in this disk than in D100R20. This reflects the fact that the vortex state is more stable against the in-plane magnetic field than that of an onion state. The large switching field is yet another example of the configurational stability effect discussed earlier, and this time the configuration is of a vortex state. It should be mentioned that this type of hysteresis has already been observed by many research groups (e.g., Refs. 4, 13, and 17).

### C. Transition involving twisted onion states

In thicker disks, the twisted onion configuration may be more stable than the normal onion in some field range. For example, the reversal process in D200R2 passes through the transition from a normal to twisted onion state at about 176 mT, leading to an abrupt change in both the projected magnetization and the spread function value. As shown in Fig. 5, the transition saves stray field energy, but it is done at the cost of both exchange and Zeeman energies, though the net change in the total energy is negligible in this transformation. Further decrease in the field leads to another configurational transition from the twisted onion to an out-of-plane vortex state at 132 mT field. The vortex state is eventually annihilated at $-158$ mT field to a twisted onion configuration, which then *continuously* evolves to that of a normal onion state. It is interesting to note that the transition from normal to twisted onion state occurs abruptly, while the reverse pro-

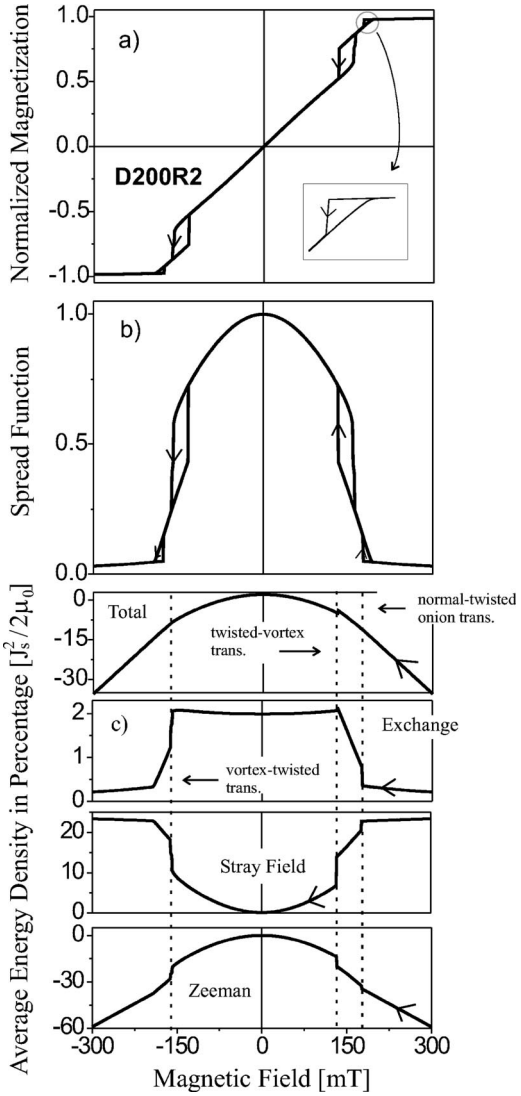


FIG. 5. The magnetization process, observed in D200R2 (diameter=200 nm, diameter-to-thickness ratio $d/t=2$), involves twisted onion states. A detailed description of the figures can be found in the caption of Fig. 2.

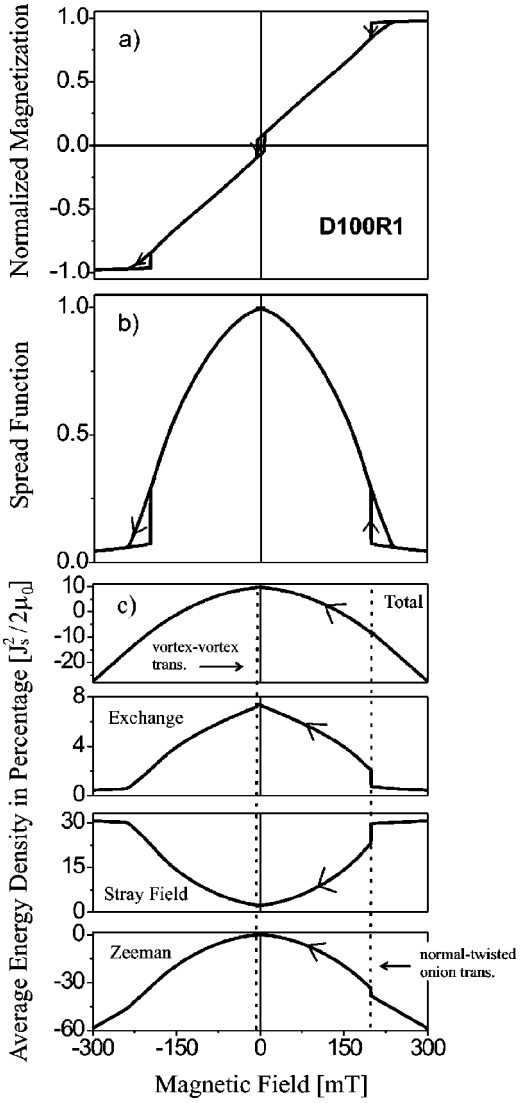


FIG. 6. The magnetization process involves in-plane vortex states. It is observed in D100R1 (diameter=100 nm, diameter-to-thickness ratio $d/t=1$). A detailed description of the figures can be found in the caption of Fig. 2.

cess, that is, transition from twisted to normal onion state, happens smoothly. This could be a numerical artifact. One piece of evidence supporting this interpretation is the total energy of the system showing a rather smooth transition, suggesting that the difference in the total energy between the two states is negligible. And the computer algorithm is programmed to always keep the *status quo* configuration, unless the energy difference is larger than that specified in the tolerance parameter.

#### D. Transitions between twisted and in-plane vortex states

Instead of going from a twisted onion to an out-of-plane vortex state, the magnetization reversal in D100R1, as shown in Fig. 6, evolves *continuously* to an in-plane vortex state with decreasing magnetic field. The continuity of the transition is evident by the smoothness in both the magnetization and spread function curves. Naturally, the core axis lies in the field direction because of the Zeeman energy term. Unlike an out-of-plane vortex state, the core of the in-plane vortex remains stationary but its core area shrinks, as the magnetic field decreases in strength. The reason for the shrinkage is simple: the smaller the core area is, the fewer surface magnetic poles are present and hence the lower the stray field energy is. At $-7$ mT, the vortex switches its polarity to align with the magnetic field, as driven by the lowering of the Zeeman energy. Further decrease in the field results in the vortex transforming back to a twisted onion which then eventually leads to a normal onion state at about $-240$ mT, all of which occur in a continuous manner with no visible diskontinuity in the magnetization, spread function, and energy curves. In agreement with that discussed in the previous paragraph, the transition from a normal to twisted onion state also occurs abruptly, this time at about 198 mT, but that from a twisted to normal is continuous, for the same reason as that discussed before. Snap shots of the

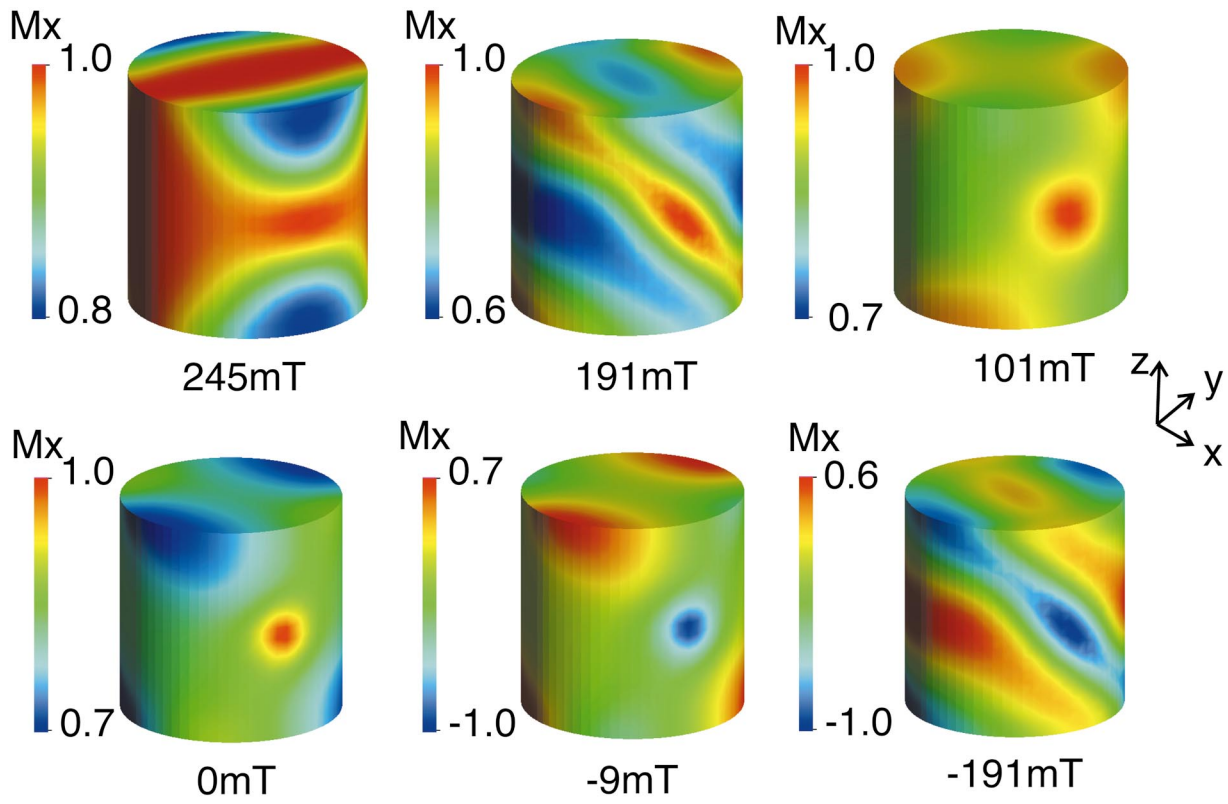


FIG. 7. (Color) Stable magnetic configurations at different magnetic fields during the magnetization process in D100R1 (diameter $=100$ nm, diameter-to-thickness ratio $d/t=1$).

magnetic configurations at various different field strengths are shown in Fig. 7 to give the reader a more visual picture of the magnetization process. Last, as far as we know, there have been no reports on magnetization processes involving in-plane vortex states in the literature.

### E. Reversal involving buckle states

For larger disks (with diameter larger than 200 nm), intermediate buckle states are (meta)stable, and transitions between an onion to a buckle state often occur. For example, Fig. 8 shows the hysteresis loop of D500A50, which passes the transition from a normal onion to a *C* state at 1.6 mT. As the field decreases to $-2.8$ mT, the *C* state switches its ''polarity'' by rotating the whole configuration by 180° while its rotation sense of the magnetization stays intact. Eventually, the *C* state is annihilated back to a normal onion state at $-8.2$ mT. It is interesting to note that the *C* state in this particular disk does not evolve into a vortex state although their structures are arguably similar: A *C* state can be viewed as that of a virtual vortex with its core sitting slightly outside the disk perimeter.

Figure 9 shows the magnetization loop of D500R30. In this disk, the normal onion state drops instead to an *S* state at 6.5 mT, which then collapses to an out-of-plane vortex state at 2 mT. Transitions to higher-order buckle states (e.g., *W* state[12]) can also be observed in thicker disks of the same diameter such as D500R5, but they are not discussed here in this paper.

## VI. EVOLUTION OF MAGNETIZATION LOOPS ON DISK SIZE

So far, hysteresis loops of different shapes (e.g., square- and dumbbell-looking loops) have been presented. Their differences are due to the degree of stability of the different magnetic configurations against the external magnetic field. But no words have yet been uttered about the evolution of the various loops. How does one evolve to another as a function of disk size, for example? In this section, we focus our attention on this issue and restrict our investigation to only the D200R series, namely, a series of disks of different thicknesses but of the same diameter fixed at 200 nm. The D200R series is singled out for the discussion because it is simple and at the same time provides some insight into the thickness dependence of the different hysteresis loops.

Figure 10 shows the dependence of the magnetization and spread value on the disk aspect ratio $d/t$ at zero field. The plot is divided into three subregions. In region I, that is, in the regime of very thin disks or large $d/t$ ratio, the hysteresis loop is square looking like that shown in Fig. 2, with essentially unity remanence and zero remanent spread value. This is expected, because there is not much of a driving force to have a closed flux configuration. In region III, that is, in the regime of low aspect ratio or of thick disks, the onion state transforms to a vortex state before it is emerged to another onion state of opposite polarity. This passage is expected because the need to avoid surface poles at the perimeter is more pressing. An example of such a hysteresis loop—a

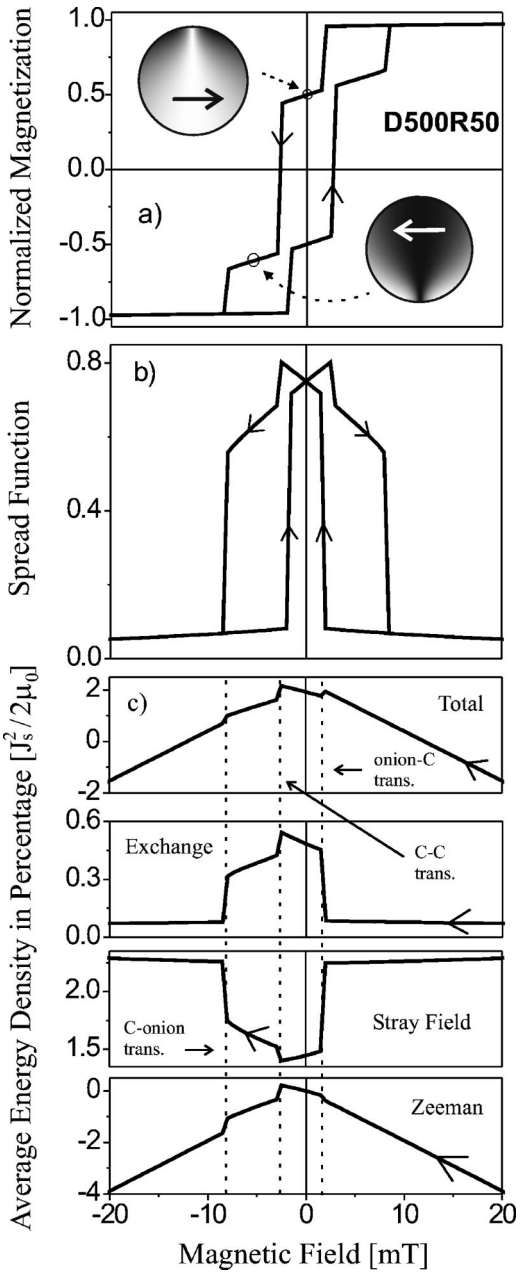


FIG. 8. D500R50 (diameter=500 nm, diameter-to-thickness ratio $d/t=50$). The magnetization process involves the *C* state. The two insets are the density plots of the *x* component of the magnetization at 0 and $-6.5$ mT field. A detailed description of the figures can be found in the caption of Fig. 2.

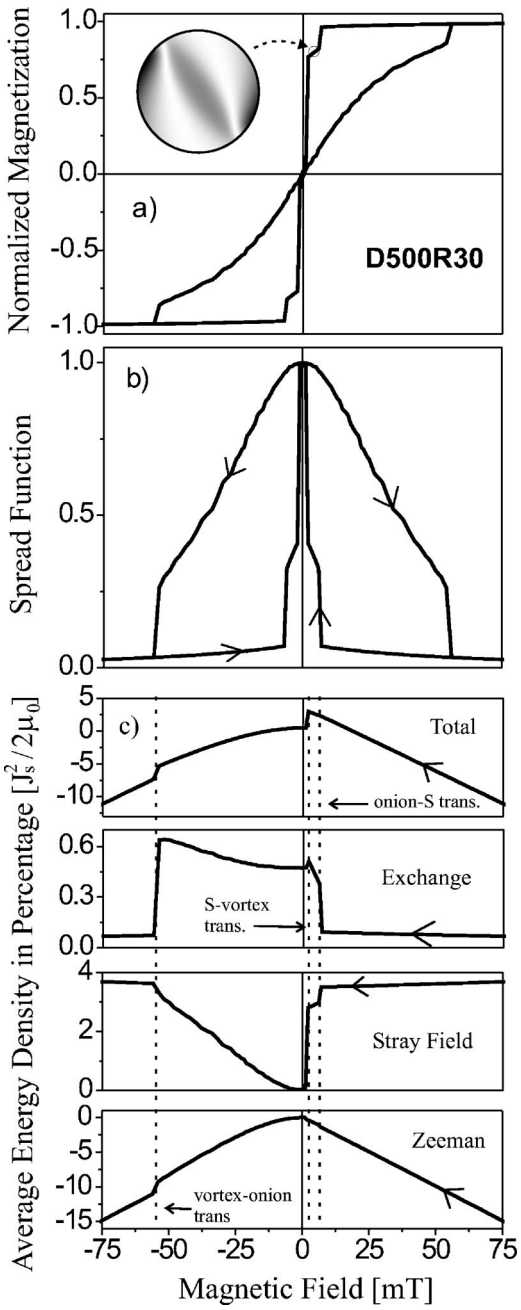


FIG. 9. The magnetization process, observed in D500R30 (diameter=500 nm, diameter-to-thickness ratio $d/t=30$), involves the *S* state. The inset is the density plot of the *x* component of the magnetization at 3 mT field. The white color corresponds to $m_x=1$, the black color $m_x=-1$. A detailed description of the other plots can be found in the caption of Fig. 2.

dumbbell-looking loop—can be seen in Fig. 4. For disks of intermediate thickness or aspect ratio, that is, those belonging to regime II as marked in the diagram, the onion state typically goes through some buckle state before it switches. The buckle state is of the *C* configuration in this particular series.

### VII. IN-PLANE ROTATIONAL FIELD

Our discussion on magnetization reversal has thus far been restricted to that with a fixed-directional magnetic field. There, it is found that a sizable field is often needed to switch the magnetization of an isotropic permalloy disk due to the configurational stability effect. But a magnetic configuration that is stable against a fixed-directional field may not be so against a rotational field. For example, if an external field is applied at an infinitesimal angle away from the symmetry axis of an onion state, it seems reasonable to suppose that the magnetization would simply undergo a slight rearrangement to arrive at a new onion state whose onion axis lies parallel

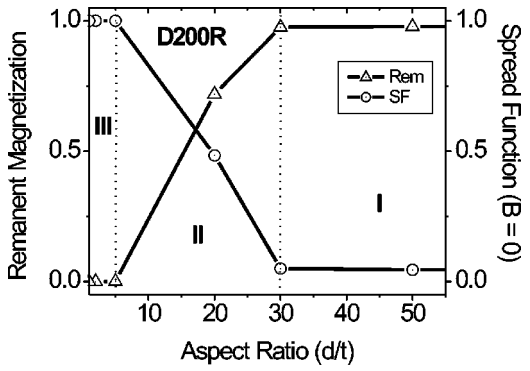


FIG. 10. Remanent magnetization and spread function at zero field are plotted as a function of the aspect ratio of the D200R series (disks whose diameter is 200 nm). Region I has a squarelike loop (see Fig. 2); the magnetization loop in region II passes through a *C* state (see Fig. 8); that in region III passes through a vortex state (see Fig. 4).

to the field direction. The transition between these two onion states has essentially no barrier in the limit that the angle between the field and onion axis approaches zero. From this realization, it can be expected that an onion state can be reversed quite effortlessly with an in-plane rotational field, as long as the rotation is smooth (by having small step size) and the rotational frequency is sufficiently low to allow the onion axis to follow closely. Using a field of the form

$$\vec{H} = H_0(\hat{x}\cos\phi + \hat{y}\sin\phi), \tag{2}$$

where $\phi$ is the angle between the external field direction and $x$ axis, and $H_0$ its amplitude, simulations of the reversal processes for D100R20 and D100R2 have been performed, and the results are shown in Fig. 11. The precise procedure of the simulations is as follows: the magnetization is first saturated by a sufficiently large in-plane field. It then decreases gradually to 5 mT for D100R20 and to 80 mT for D100R2, from which the field begins to rotate in the manner as prescribed by the above equation with the step size $\Delta\phi = 5°$. The onion state is stable in these two disks at the respective field strengths mentioned above. The facts that the magnetization along the field direction stays constant and its $x$ component follows a cosine curve as $\phi$ increases from 0 to 180° suggest that the onion axis practically follows the field. Needless to say, the onion state is reversed when the angle $\phi$ reaches 180°. Note that there is negligible hysteresis present in the loop, as can be expected from a barrierless process. If a fixed-directional field were used instead, much larger fields (18 mT for D100R200 and 120 mT for D100R2, as discussed earlier) would have been needed to reverse the magnetization. For D100R20, a much smaller field strength (less than 1 mT) can also be used because the onion configuration is stable or metstable even at remanence. But for D100R2, there is a minimum field strength below which this rotational field method cannot be used for the magnetization reversal. The reason is simply that the onion state is unstable below 50 mT field and collapses into a vortex state.

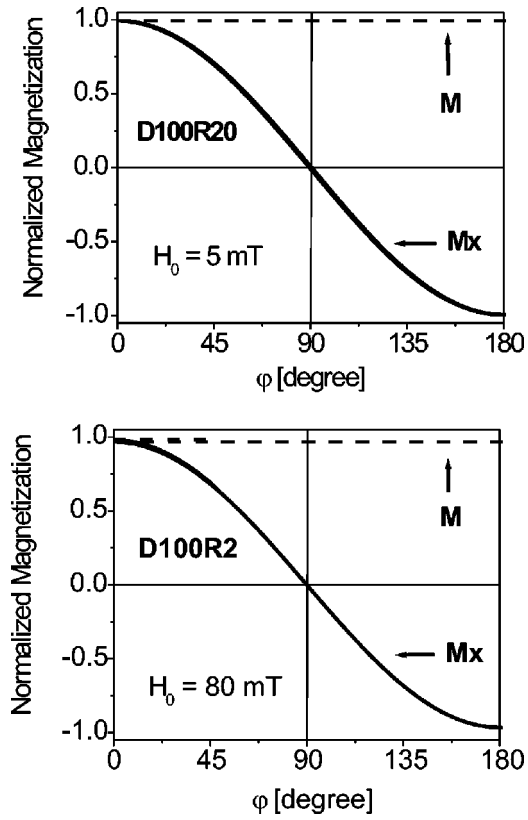


FIG. 11. The $x$ component of the magnetization and that along the field direction are plotted as a function of the field angle $\phi$ in degrees for D100R20 and D100R2 (i.e., disks whose diameter is 100 nm, diameter-to-thickness ratio $d/t = 20$ and 2, respectively). $H_0$ is the amplitude of the rotational field.

## VIII. DISCUSSION AND SUMMARY

Perhaps the discussion should begin by emphasizing that the simulations performed in this study are based on a static approach. No words have been and can be said about the way and the speed at which the magnetization evolves from one (meta)stable configuration to another. Such information can only be obtained or theorized using a dynamical approach, such as that uses the Gilbert equation.[18] Recently, some aspect of the transient states during the switching process has been addressed by Fidler et al. in Ref. 19.

The present investigation makes it clear that the magnetization processes in these submicron disks are driven solely by the stability of the magnetic configuration in which the disk finds itself in, and not by wall displacement or unison rotation of the magnetization, as is often the case in bulk samples. And for this reason, we feel that the so-called configurational anisotropy would have been more accurately named configurational stability, for this effect is not of anisotropy in origin. If it were, a simple rotational field, such as that discussed in the previous section, would not have been successful in avoiding its effect in the reversal process.

We are pleasantly surprised by the sensitivity of the spread function in tracking the degree of nonuniformity in a magnetic configuration. This is evident by the fact that it has a rather smooth dependence on the field strength in all of the

reversal processes studied in this paper. Further, it provides useful information about the evolution of a magnetic configuration, as that illustrated in the case of an onion state becoming more or less onionated by the action of the magnetic field.

Although no vortex state is observed in many thinner disks such as D100R20, it does not mean that a vortex state is not stable in these elements. Indeed, our numerical simulation shows that most of these elements would have favored a vortex state, provided such a state is accessible in the reversal path.

In summary, the magnetization processes of permalloy disks of different sizes have been studied. It is found that these processes are governed by the stability of the magnetic states. Many different types of hysteresis loops have been observed due to the many different metastable and stable states the disk finds itself in. In some cases, an in-plane rotational field has been successfully employed to reverse the magnetization and avoid the configurational stability of the magnetic state.

## APPENDIX: THE SPREAD FUNCTION

It is the intention of this appendix to show that the spread function is inclusively bounded in the interval [0,1]. The function can be formally defined as follows:

$$SF = 1 - \left| \frac{1}{V} \sum_{i=1}^{N} \vec{m}_i v_i \right|^2 = 1 - \langle m_x \rangle^2 - \langle m_y \rangle^2 - \langle m_z \rangle^2, \tag{A1}$$

where $N$ is the number of nodes used in the simulation, $\vec{m}_i$ the normalized magnetization vector in the $i$th node, and $v_i$ its corresponding volume. Here, we assign a volume to each node in such a way that the sum of the nodal volumes is the total volume of the sample; that is, $V = \Sigma_i^N v_i$ the volume of the sample. From Eq. (A1), it is clear that SF must be less than 1 because $\langle m_x \rangle^2$, $\langle m_y \rangle^2$, and $\langle m_z \rangle^2$ are positive numbers. The first question is, does it include 1? To prove this, it is sufficient to show a magnetic configuration in which SF $=1$. One such a configuration can be as simple as that of a particle with two domains of equal size but pointing in opposite directions, say, in the $x$ direction. Then, $\langle m_x \rangle = 0$, which implies that $\langle m_x \rangle^2 = 0$. Therefore, SF$=1$ in this simple example.

To show that SF$\geqslant 0$, we rewrite Eq. (A1) as follows:

$$\begin{aligned} SF &= 1 - \left( \frac{1}{V} \sum_{i=1}^{N} \vec{m}_i v_i \right) \left( \frac{1}{V} \sum_{j=1}^{N} \vec{m}_j v_j \right) \\ &= 1 - \frac{1}{V^2} \sum_{i=1}^{N} \sum_{j=1}^{N} v_i v_j \cos\theta_{ij}, \end{aligned} \tag{A2}$$

where $\theta_{ij}$ is the angle between the moment vectors at node $i$ and $j$. Because

$$\begin{aligned} \frac{1}{V^2} \sum_{i=1}^{N} \sum_{j=1}^{N} v_i v_j \cos\theta_{ij} &\leqslant \frac{1}{V^2} \sum_{i=1}^{N} \sum_{j=1}^{N} v_i v_j |\cos\theta_{ij}| \\ &\leqslant \frac{1}{V^2} \sum_{i=1}^{N} \sum_{j=1}^{N} v_i v_j = 1, \end{aligned}$$

it follows that SF$\geqslant 0$. The fact that SF includes zero can be seen by examining its value for a single-domain particle.

*Permanent address: Max-Planck-Institut für Mikrostrukturphysik, Weinberg 2, 06120 Halle, Germany. Electronic address: kha@mpi-halle.mpg.de

[1] M.E. Schabes and H.N. Bertram, J. Appl. Phys. **64**, 1347 (1988).
[2] S. Chikazumi, *Physics of Ferromagnetism*, 2nd ed. (Oxford Science, Oxford, 1997).
[3] Y. Zheng and J.-G. Zhu, J. Appl. Phys. **81**, 5471 (1997).
[4] R.P. Cowburn, D.K. Koltsov, A.O. Adeyeye, M.E. Welland, and D.M. Tricker, Phys. Rev. Lett. **83**, 1042 (1999).
[5] A. Hubert and R. Schäfer, *Magnetic Domains: The Analysis of Magnetic Microstructures* (Springer, Berlin, 1998).
[6] P. Allia, *Basic Concepts of Ferromagnetism: A Primer* (World Scientific, Singapore, 1996), Chap. 1, p. 1.
[7] J. W. F. Brown, *Micromagnetics* (Interscience, New York, 1963).
[8] J.-G. Zhu, Y. Zheng, and G.A. Prinz, J. Appl. Phys. **87**, 6668 (2000).
[9] J. Ferré, *Dynamics of Magnetization Reversal: From Continuous to Patterned Ferromagnetic Films*, Vol. 83 of *Topics in Applied Physics*, edited by B. Hillebrands and K. Ounadjela (Springer, Berlin, 2002), Chap. 5, p. 127.
[10] D.R. Fredkin and T.R. Koehler, IEEE Trans. Magn. **26**, 415 (1990).
[11] R. Hertel, J. Appl. Phys. **90**, 5752 (2001).
[12] J. K. Ha, R. Hertel, and J. Kirschner, Phys. Rev. B (to be published).
[13] K.Y. Guslienko, V. Novosad, Y. Otani, H. Shima, and K. Fukamichi, Phys. Rev. B **65**, 024414 (2001).
[14] M.E. Schabes, J. Magn. Magn. Mater. **95**, 249 (1991).
[15] A. Hubert and W. Rave, Phys. Status Solidi B **211**, 815 (1999).
[16] J.G. Deak and R.H. Koch, J. Magn. Magn. Mater. **213**, 25 (2000).
[17] I.L. Prejbeanu, M. Natali, L.D. Buda, U. Ebels, A. Lebib, Y. Chen, and K. Ounadjela, J. Appl. Phys. **91**, 7343 (2002).
[18] T.L. Gilbert, Phys. Rev. **100**, 1243 (1955).
[19] J. Fidler, T. Schrefl, W. Scholz, D. Suess, and V.D. Tsiantos, Physica. B **306**, 112 (2001).
[20] J. Rothman, M. Klaui, L. Lopez-Diaz, C. Vaz, A. Bleloch, J. Bland, Z. Cui, and R. Speaks, Phys. Rev. Lett. **86**, 1098 (2001).
[21] Of course, regular domains are also seen in patterned thin films if the patterns are large (50 times the exchange length or more).
[22] Note that Rothman *et al.* (Ref. 20), have also used the term onion state to describe a similar state in ring-shaped elements.